HHS Public Access

Author manuscript

Int J Min Sci Technol. Author manuscript; available in PMC 2021 February 16.

Published in final edited form as:

Int J Min Sci Technol. 2020 April ; 30(4): 449–454. doi:10.1016/j.ijmst.2020.05.002.

Diesel and welding aerosols in an underground mine

Aleksandar D. Bugarski[*], **Teresa L. Barone**, **Jon A. Hummer**

National Institute for Occupational Safety and Health, Pittsburgh Mining Research Division, Pittsburgh, PA 15236, USA

Abstract

Researchers from the National Institute for Occupational Safety and Health (NIOSH) conducted a study in an isolated zone of an underground mine to characterize aerosols generated by: (1) a diesel-powered personnel carrier vehicle operated over a simulated light-duty cycle and (2) the simulated repair of existing equipment using manual metal arc welding (MMAW). Both the diesel-powered vehicle and MMAW process contributed to concentrations of nano and ultrafine aerosols in the mine air. The welding process also contributed to aerosols with electrical mobility and aerodynamic mobility count median diameters of approximately 140 and 480 nm, respectively. The welding particles collected on the filters contained carbon, iron, manganese, calcium, and aluminum.

Keywords

Diesel aerosols; Welding aerosols; Underground mining; Size distribution

1. Introduction

Diesel-powered vehicles have been one of the primary sources of nano (D_{50} < 50 nm) and ultrafine (D_{50} < 100 nm) aerosols in underground mines [1–5]. The physical and chemical properties of these aerosols are a function of numerous factors, including fuel and lubricating oil properties, engine design, engine operating conditions, and exhaust aftertreatment [3]. The primary constituents of aerosols emitted by engines that are not equipped with diesel particulate filter (DPF) systems are elemental carbon, sulfates, nitrates, ash, and hundreds of different free or particle-bound organic compounds of varying volatility [6–8]. DPF-equipped diesel engines emit primarily sub-30-nm nucleation mode aerosols that are composed mainly of sulfates and organic compounds [7,8]. In terms of size, diesel aerosols are typically polydisperse and log-normally distributed in one, two, or even three distinctive modes [7–9].

[*]Corresponding author. abugarski@cdc.gov (A.D. Bugarski).

Because long-term exposure to diesel exhaust has been linked to various adverse pulmonary, cardiovascular, and other health outcomes, occupational exposure to diesel aerosols is a major health concern for underground mining operators and regulators [10–15]. Currently, the exposure of underground metal and nonmetal miners to diesel particulate matter (DPM) in the U.S. is limited by Mine Safety and Health Administration (MSHA) regulations to 160 $\mu g/m^3$ [16]. In 2012, the International Agency for Research on Cancer (IARC) classified diesel exhaust as a Group 1 carcinogen [17,18]. The regulatory efforts to reduce emissions from diesel engines resulted in major improvements in engine combustion technologies, exhaust aftertreatment technologies, and alternative fuels [19–28]. The implementation of advanced engine, exhaust aftertreatment and fuel technologies could be instrumental to the underground mining industry's efforts to reduce exposures to DPM and diesel exhaust gases. Monitoring accurate and reliable exposures to DPM is still one of the major challenges [11].

Other potential sources of submicron aerosols in underground mines are various welding processes that are used to fabricate and repair metal products. Welding processes generate aerosols, also known as welding fumes, in a wide size range from a few nanometers to several microns [29–31]. Welding processes can generate locally high concentrations of aerosols, between 100 and 400 mg/m^3 [29,32]. Direct ejection of spherical micro-spatter from the electrodes, nucleation and condensation of gas-phase metals to form primary particles, and coagulation of primary particles to form agglomerates are recognized as primary mechanisms for the generation of welding aerosols [32]. In mixtures with carbonaceous particles, transition metals mediate the production of reactive oxygen species, and therefore increase oxidative damage and inflammation [33–36]. In 2017, the International Agency for Research on Cancer (IARC) classified welding fumes as a Group 1 carcinogen [37,38].

Due to their portability, methods that utilize flux-coated electrodes, such as manual metal arc welding (MMAW) or stick welding, may be more suitable for mobile applications in underground mines than methods that employ an inert gas shield and require the use of compressed gas. The MMAW method tends to generate aerosols in higher concentrations and in larger sizes than processes that use an inert gas shielding [32]. The composition of MMAW aerosols depends on the compositions of the flux, electrode, and welded metal [29,39]. Depending on the composition of flux material, MMAW aerosols may contain calcium (Ca), sodium (Na), fluo-ride (F), aluminum (Al), potassium (K), silicon (Si), and titanium (Ti). Depending on the composition of the electrode and welded metals, these can contain iron (Fe), manganese (Mn), nickel (Ni), and chromium (Cr). In the U.S., the exposure of underground metal and nonmetal miners to individual metal oxides present in welding fumes is limited by MSHA to the 1973 American Conference of Governmental Industrial Hygienists (ACGIH) threshold limit values (TLVs) for these compounds [40,41].

2. Methods

The current study was designed to characterize aerosols found in underground mines downwind from a light-duty diesel-powered vehicle operated over a simulated cycle and downwind of the simulated process of MMAW performed by an experienced welder to repair or modify existing equipment outside of well-ventilated designated welding spaces.

The experimental work in this study was executed using an isolated zone methodology [42]. This methodology was used to characterize aerosols that contributed to the underground environment by: (1) a light-duty diesel-powered vehicle and (2) the MMAW process. This methodology allowed for achieving reasonable repeatability and accuracy while preserving the genuineness of testing under prevailing ambient conditions.

The layout of the isolated zone test site used for these tests is shown in Fig. 1. All drifts within the test site were 6.1 m wide and 2.7 m high. The stoppings were used to isolate the zone from the adjacent areas of the mine. A 610-mm-diameter exhaust duct was sealed in the stopping constructed at the downstream end of the zone (Fig. 1).

The zone was ventilated with air supplied from the main ventilation shaft. A stable flow rate through the zone was maintained with a two-stage fan (Model 60×2–30–3600 CR FP by Spendrup Fan Co.). The fan was installed in the exhaust duct upstream of a permanent stopping. A stainless-steel pitot airflow traverse probe (VOLU-probe/SS from Air Monitor Corporation) was inserted upstream of the fan and was used to continuously measure airflow through the duct. The Digiquartz Portable Standard Model 765 (Paroscientific, Inc.) pressure transducer was used to measure differential pressure across the pitot probe. The average airflow rates for diesel and welding tests were (5.42 ± 0.07) m^3/s and (5.34 ± 0. 08) m^3/s, respectively. Since the intra- and inter-test variabilities in the flow rates were<2% of targeted values, all concentrations were reported as those at the prevailing ventilation rates. To minimize contamination, the experimental work was scheduled during the night hours when the diesel-powered traffic and welding activities in the drifts leading from the main ventilation shaft to the zone were lower than those observed during the daytime hours. Dust entrainment from the roadways leading to the zone and in the zone was suppressed by applying a water/oil dust emulsion.

A light-duty personnel carrier vehicle, powered by a naturally aspirated, mechanically controlled diesel engine (Table 1), was the primary source of diesel aerosols during the diesel test. The vehicle was driven by a single operator in the 150-m section of the main drift, between the upstream turning point (UTP) and downstream turning point (DTP) (Fig. 1) at speeds of up to 24 km/hr. The operator was doing simple three-point turns at the UTP and DTP. The selected properties of the ultralow sulfur diesel (ULSD) fuel used by the tested vehicle are shown in Table 2.

It is important to note that the study was conducted at approximately 1500 m above sea level and that the reduced availability of oxygen (O_2) might have adversely affected the emissions from the naturally aspirated diesel engine or welding process. It is also important to note that the contributions of the whole vehicle rather than just the engine were assessed in this study. Therefore, aerosols at the downstream measurement and sampling station (DMSS) potentially include not only the aerosols emitted via tail-pipe but also those aerosols emitted via crankcase breather and/or those leaked from the engine systems.

A diesel-powered welder/generator (Big Blue 300 Pro from Miller Electric) was used to perform MMAW welding. In order to eliminate the contribution of the diesel engine in the welding system to the concentrations of aerosols at DMSS, the utility truck with the welder

was parked in an adjacent crosscut behind the sealed curtain and was ventilated via a different ventilation circuit. The experienced welder worked on the workbench located in the middle of the main drift at the location (Fig. 1). He welded a mild steel plate using an iron powder, low hydrogen electrode. With exception of the short 10-second periods needed to replace the electrodes, he was welding continuously throughout the whole test.

The measurements and sampling were performed at two locations–the upstream measurement and sampling station (UMSS) and the downstream measurement and sampling station (DMSS)—shown in Fig. 1. The UMSS was located at the upstream end of the isolated zone, 50 m upwind of the UTP, and the DMSS was located between 230 and 250 m downwind of the DTP. The results of measurements and sampling performed at the UMSS were used to quantify background concentrations of criteria pollutants and, if necessary, to correct for background concentrations of the targeted pollutants.

The size distribution and number concentrations of aerosols were measured at the DMSS with a Fast Mobility Particle Sizer (FMPS) spectrometer (Model 3091 by TSI) and an Electrical Low Pressure Impactor (ELPI by Dekati) [43–45]. The second FMPS spectrometer was used to measure the size distribution and number concentrations of aerosols at the UMSS. The FMPS and ELPI were previously recommended and used to characterize diesel aerosols or welding fumes in occupational settings [39,46–50]. The FMPS measures the number concentrations and size distributions of aerosols with an electrical mobility diameter between 6 and 560 nm. The instrument was factory calibrated and zero was checked using HEPA filter at the inlet to the instrument before each of the measurements. The ELPI measures concentrations and size distributions of aerosols with aerodynamic mobility diameters between 5 and 10000 nm. The 25-mm greased aluminum foils were used as the substrates. The instrument was factory calibrated and zeroed before each of the measurements. The inlet ports for the FMPS and ELPI were mounted on the head of a rotating sampling system that allowed for the collection of integrated aerosol samples along the perimeter of the circle defined by the center of rotation, approximately 1.82 m from the ground with a 0.91-m radius. The sampling head rotated at approximately 1 rpm, which translated into a sampling head angular speed of approximately 100 mm/s. The FMPS size distributions were fitted with lognormal curves using DistFit software [51].

Elemental carbon (EC) analysis was performed on triplicate sub-micron aerosol samples collected at the UMSS and DMSS. The samples were collected on tandem 37-mm quartz fiber filters (QFFs) enclosed in diesel particulate matter cassettes (Model 225–317 by SKC, Eighty Four, PA) using a custom-designed sampling system [52]. The 10-mm Dorr-Oliver cyclones (Model 456,243 by Zefon International) were used as a pre-classifier to eliminate the majority of coarse aerosols from the submicron and respirable samples. A nominal sampling flow rate of 1.7 lpm was maintained for all samples using subsonic critical orifices, installed in the manifolds coupled to a single vacuum pump (Sogevac SV25B by Oerlikon Leybold Vacuum GmbH). Since, as a result of thorough mixing along the long mine drifts, the aged submicron aerosols were uniformly distributed across the opening at the UMSS, the sampling and instrument inlets were mounted on a stationary tripod. At the DMSS, where mixtures of the aged and freshly generated aerosols were not uniformly distributed across the opening, the sampling and instrument inlets were mounted on a rotating head. The actual

sampling flow rates were determined using results of flow verifications with a primary flow calibrator (Bios Defender 530 by Mesa Laboratories).

The sampling occurred over 7200-second periods. The size distribution and number concentrations of aerosols were concurrently measured using the FMPS and ELPI. However, the results of measurements with the FMPS at the DMSS and UMSS and with the ELPI at the DMSS were analyzed only for selected 1200-second (20-minute) periods of the diesel and welding tests. The periods were selected to minimize the effects of initial transition processes (2400 s in the test) and background contamination. The results of FMPS measurements at the UMSS and DMSS were temporally aligned to account for time needed for contaminants to migrate from the UMSS to DMSS. The time delay was estimated from air velocity and distance measurements and verified using selected concentration spikes.

A thermo-optical transmittance (TOT) analysis was performed using a carbon analyzer (Model Lab OC-EC Aerosol Analyzer by Sunset Laboratory Inc., Portland, Oregon) and following NIOSH Method 5040 protocols [53]. An analysis of welding aerosol elemental composition was performed on QFF media punched out from sampling and blank filters that underwent TOT analysis. The filters were analyzed by scanning electron microscopy (SEM) (Model S-4800 by Hitachi, Tokyo, Japan) and energy dispersive x-ray spectroscopy (EDS) (by Bruker Quantax, Madison, Wisconsin). The elemental analysis was done using 20-kV incident beam energy, and the particle imaging was done at 5 kV.

3. Results and discussion

3.1. Concentrations of aerosols

Normalized number concentrations of aerosols measured with the FMPS at the DMSS and UMSS and with the ELPI at the DMSS are shown in Fig. 2a and b, respectively. The concentrations shown were normalized with the highest concentrations observed during these periods. The concentrations of aerosols at the DMMS exhibited quasi-steady trends (Fig. 2a and b). For the duration of the welding test and during the second part of the diesel test, the FMPS measurements at the UMSS suggest consistent light activity of diesel-powered vehicles in the other parts of the mine on the fresh air path to the zone. For diesel and welding tests, the FMPS-measured number concentrations of the sub-500 nm aerosols at the UMSS were on average 13% and 20% of the corresponding concentrations at the DMSS, respectively. For the welding test, the dependence of the number concentrations on the position of sampling inlet indicates incomplete mixing and potential aerosol and plume stratification. The dependence on the position of the sampling inlets was much less pronounced for the diesel test (Fig. 2a and b). For the conditions generated, the concentrations of aerosols produced by the welding process were approximately one order of magnitude lower than those generated by the light-duty diesel-powered vehicle.

3.2. Size distribution of aerosols

The normalized FMPS and ELPI size distributions of aerosols at the DMSS for selected time instances of the diesel and welding tests are shown in Fig. 3a and b, respectively. The concentrations shown were normalized with the highest peak concentrations observed during

these test periods. The size distributions are shown for selected instances of the low (LOW) and high (HIGH) total number concentrations. For the diesel test, FMPS-measured aerosols with electrical mobility count median diameters (CMDs) below 500 nm were predominantly distributed between nucleation and agglomeration modes (Fig. 3a and Table 3). For the welding test, FMPS-measured number distributions indicated the presence of additional agglomeration mode with electrical mobility CMDs around 140 nm (Fig. 3a and Table 3). In the case of the welding test, the ELPI that has a wider measurement range than FMPS showed aerosols in the mode centered on the ELPI stage with aerodynamic CMDs of 483 nm (Fig. 3a and b). The ELPI results indicate that the number concentrations of aerosols at the micron stages of the ELPI were low (Fig. 3b). Table 3 summarizes the statistical parameters for the lognormal curves fitted to the FMPS distributions shown in Fig. 3a.

3.3. Chemical composition

The relative contributions of the studied processes to submicron EC mass concentrations are shown in Fig. 4. The concentrations were normalized with respect to the highest of the concentrations observed for these tests and were averaged for the triplicate samples. Submicron EC was detected for both cases. For the generated conditions, the contribution of the welding process to submicron EC concentrations was found to be one order of magnitude lower than that of the diesel-powered vehicle (Fig. 4).

The elemental composition of submicron aerosols was analyzed following TOT analysis, and the SEM images and EDS spectra are shown in Fig. 5. The SEM images of the fibers on the blank filter and on the fibers of the post-TOT-analysis filter used to collect sub-micron aerosols during the diesel test showed an absence of metallic aerosols on the fibers. The EDS analysis of these filters showed only the presence of Si and O_2 from the filter media. The SEM images for the post-TOT-analysis filters for the welding test show particles attached to the fibers. The compact morphology may have resulted from sintering during the high-temperature (800–900 ℃) interval of TOT analysis. The EDS analysis of particles on the filters collected during the welding test showed the presence of Fe, Mn, Ca, and Al. The Fe and Mn are most likely from welding base and electrode metals, while the Ca and Al are probably from the flux material coating the electrode.

4. Conclusion

The isolated zone study was used to characterize the physical and chemical properties of aerosols emitted in an underground mine by a light-duty personnel carrier vehicle operated over a simulated light-duty cycle and a manual metal arc welding (MMAW) process. The aerosols contributed by the diesel-powered vehicle to the underground environment were found to be predominantly distributed between a nucleation mode with an electrical mobility count median diameter (CMD) of around 15 nm and an accumulation mode with a CMD of about 70 nm. Nano and ultrafine aerosols of similar size were found in the mine environment downwind of the studied MMAW process. However, welding aerosols were also found in an accumulation mode with an electrical mobility of 140 nm and an aerodynamic mobility CMD of approximately 480 nm. Neither the diesel engine nor welding process produced measurable number concentrations of micron-size aerosols. The

energy dispersive x-ray spectroscopy (EDS) analysis showed that welding particles collected on the filters contained Fe, Mn, Ca, and Al. The particular welding process examined in this study contributed less to number and elemental carbon concentrations than the light-duty diesel vehicle. The fact that the welding and diesel aerosols are both sub-micron in size pose potential challenges to sampling methodologies currently used to assess the exposure of underground miners to diesel particulate matter. It is important to note that data obtained in this study are limited in the scope and additional work is needed to further characterize aerosols emitted by a variety of diesel-powered vehicles and welding processes in the underground environment.

Acknowledgement

This research was internally funded by NIOSH.

References

[1]. Saarikoski S, Teinilä K, Timonen H, Aurela M, Laaksovirta T, Reyes F, et al. Particulate matter characteristics, dynamics and sources in an underground mine. Aerosol Sci Technol 2018;52(1):114–22.

[2]. Debia M, Couture C, Njanga P-E, Neesham-Grenon E, Lachapelle G, Coulombe H, et al. Diesel engine exhaust exposures in two underground mines. International Journal of Mining Science and Technology 2017;27(4):641–5.

[3]. Bugarski AD, Janisko S, Cauda EG, Noll JD, Mischler SE. Controlling exposure - diesel emissions in underground mines. Society for Mining, Metallurgy, and Exploration; 2012.

[4]. Bugarski AD, Cauda EG, Janisko SJ, Hummer JA, Patts LD. Aerosols emitted in underground mine air by diesel engine fueled with biodiesel. J Air Waste Manag Assoc 2010;60(2):237–44. [PubMed: 20222537]

[5]. Bugarski AD, Schnakenberg GH, Hummer JA, Cauda E, Janisko SJ, Patts LD. Effects of diesel exhaust aftertreatment devices on concentrations and size distribution of aerosols in underground mine air. Environ Sci Technol 2009;43 (17):6737–43. [PubMed: 19764243]

[6]. Zielinska B, Sagebiel J, McDonald J, Rogers CF, Fujita EM, Mousset-Jones P, Woodrow JE. Measuring diesel emissions exposure in underground mines: a feasibility study In: Proceedings of the research directions to improve estimates of human exposure and risk from diesel exhaust. Boston, MA: Health Effects Institute; 2002p.181–232.

[7]. Khalek IA, Bougher TL, Merritt PM, Zielinska B. Regulated and unregulated emissions from highway heavy-duty diesel engines complying with U.S. Environmental Protection Agency 2007 emissions standards. J Air Waste Manag Assoc 2011;61(4):427–42. [PubMed: 21516938]

[8]. Khalek IA, Blanks MG, Merritt PM, Zielinska B. Regulated and unregulated emissions from modern 2010 emissions-compliant heavy-duty on-highway diesel engines. J Air Waste Manag Assoc 2015;65(8):987–1001. [PubMed: 26037832]

[9]. Ruehl C, Herner JD, Yoon S, Collins JF, Misra C, Na K, et al. Similarities and differences between “traditional” and “clean” diesel PM. Emission Control. Science and Technology 2015;1(1):17–23.

[10]. Peters S, de Klerk N, Reid A, Fritischi L, Musk AW, Vermulen R. Quantitative levels of diesel exhaust exposure and the health impact in the contemporary Australian mining industry. Occup Environ Med 2017;74(4):282–9. [PubMed: 27919060]

[11]. Chang P, Xu G. A review of the health effects and exposure-responsible relationship of diesel particulate matter for underground mines. International Journal of Mining Science and Technology 2017;27(5):831–8.

[12]. Attfield MD, Schleiff PL, Lubin JH, Blair A, Stewart PA, Vermeulen R, et al. The diesel exhaust in miners study: A cohort mortality study with emphasis on lung cancer. J Natl Cancer Inst 2012;104(11):869–83. [PubMed: 22393207]

[13]. Silverman DT, Samanic CM, Lubin JH, Blair AE, Stewart PA, Vermeulen R, et al. The diesel exhaust in miners study: A nested case-control study of lung cancer and diesel exhaust. J Natl Cancer Inst 2012;104(11):855–68. [PubMed: 22393209]

[14]. Power MC, Weiskopf MG, Alexeeff SE, Coull BA, Avron S, Schwartz J. Traffic-related air pollution and cognitive functions in a cohort of older men. Environ Health Perspect 2011;119(5):682–7. [PubMed: 21172758]

[15]. Mills NL, Miller MR, Lucking AJ, Beveridge J, Flint L, Boere AJ, et al. Combustion-derived nanoparticulate induces the adverse vascular effects of diesel exhaust inhalation. Eur Heart J 2011;32(21):2660–71. [PubMed: 21753226]

[16]. 71 FR 36483. 30 CFR Part 57 Diesel particulate matter exposure of underground metal and nonmetal miners. Limit on concentration of diesel particulate matter Code of Federal Regulations Washington DC US Government Printing Office. Office of the Federal Register.

[17]. IARC. IARC Press Release No 213 June 12 Diesel Engine Exhaust Carcinogenic International Agency for Research on Cancer World Health Organization 2012.

[18]. IARC Working Group on the Evaluation of Carcinogenic Risks to Humans. Diesel and gasoline engine exhausts and some nitroarenes In: Proceedings of IARC monographs on the evaluation of carcinogenic risks to humans. Lyon: IARC; 2014.

[19]. US EPA. Nonroad Compression-Ignition Engines: Exhaust Emission Standards United States Environmental Protection Agency Office of Transportation and Air Quality EPA-420-B-16–02240; 2016.

[20]. EU. Regulation (EU) 2016/1628 of the European Parliament and of the Council Official. Journal of the European Union L252/3; 2016.

[21]. Lucachick G, Avenido A, Watts W, Kittelson D, Nortrop W. Efficacy of in-cylinder control of particulate emissions to meet current and future regulatory standards In: Proceedings of SAE 2014 world congress and exhibition. Detroit, MI: SAE International; 2014.

[22]. Herner JD, Hu S, Robertson WH, Huai T, Chang M-CO, Rieger P, et al. Effect of advanced aftertreatment for PM and NOx reduction on heavy-duty diesel engine ultrafine particle emissions. Environ Sci Technol 2011;45(6):2413–9. [PubMed: 21322629]

[23]. Karjalainen P, Ronkko T, Lahde T, Rostedt A, Keskinen J, Saarikoski S, et al. Reduction of heavy-duty diesel exhaust particulate number and mass at low exhaust temperature driving by the DOC and the SCR. SAE Int J Fuels Lubr 2013;5(3):1114–22.

[24]. Yoo D, Kim D, Jung W, Kim N, Lee D. Optimization of diesel combustion system for reducing PM to meet tier 4-final emission regulation without diesel particulate filter In: Proceedings of SAE/KSAE 2013 international powertrains, fuels and lubricants meeting. Seoul: SAE International; 2013.

[25]. Jeon J, Lee JT, Park S. Nitrogen compounds (NO, NO_2, N_2O, and NH_3) in NO_X emissions from commercial EURO VI type heavy-duty diesel engines with a urea-selective catalytic reduction system. Energy Fuels 2016;30(8):6828–34.

[26]. Smagala TG, Christensen E, Christison KM, Mohler RE, Gjersing E, McCormick RL. Hydrocarbon renewable and synthetic diesel fuel blendstocks: Composition and properties. Energy Fuels 2013;27(1):237–46.

[27]. Bugarski AD, Hummer JA, Vanderslice S. Effects of hydrotreated vegetable oil on emissions of aerosols and gases from light-duty and medium-duty older technology engines. Journal of Occupational and Environmental Hygiene 2016;13(4):297–306.

[28]. Bugarski AD, Hummer JA, Vanderslice SE. Effects of FAME biodiesel and HVORD on emissions from an older technology diesel engine. Min Eng 2017;69 (12):43–9. [PubMed: 29348698]

[29]. Oprya M, Kiro S, Worobiec A, Horemans B, Darchuk L, Novakovic V, et al. Size distribution and chemical properties of welding fumes of inhalable particles. J Aerosol Sci 2012;45:50–7.

[30]. Cena LG, Chisolm WP, Keane MJ, Cumpston A, Chen BT. Size distribution and estimated respiratory deposition of total chromium, hexavalent chromium, manganese, and nickel in gas metal arc welding fume aerosols. Aerosol Sci Technol 2014;48(12):1254–63. [PubMed: 26848207]

[31]. Stanislawska M, Halatek T, Cieslak M, Kaminska I, Kuras R, Janasik B, et al. Coarse, fine and ultrafine particles arising during welding - Analysis of occupational exposure. Microchem J 2017;135:1–9.

[32]. Zimmer AT, Biswas P. Characterization of the aerosols resulting from arc welding processes. J Aerosol Sci 2001;32(8):993–1008.

[33]. Valavanidis A, Salika A, Theodoropoulou A. Generation of hydroxyl radicals by urban suspended particulate air matter. The role of iron ions. Atmos Environ 2000;34(15):2379–86.

[34]. Wilson MR, Lightbody JH, Donaldson K, Sales J, Stone V. Interactions between ultrafine particles and transition metals in vivo and in vitro. Toxicol Appl Pharmacol 2002;184(3):172–9. [PubMed: 12460745]

[35]. Knaapen AM, Shi T, Borm PJA, Schins RPF. Soluble metals as well as the insoluble particle fraction are involved in cellular DNA damage induced by particulate matter. Mol Cell Biochem 2002;234–235:317–26.

[36]. Jiménez LA, Thompson J, Brown DA, Rahman I, Antonicelli F, Duffin R, et al. Activation of NF-κB by PM_{10} occurs via an iron-mediated mechanism in the absence of IκB degradation. Toxicol Appl Pharmacol 2000;166(2):101–10. [PubMed: 10896851]

[37]. Guha N, Loomis D, Guyton KZ, Grosse Y, El Ghissassi F, Bouvard V, et al. Carcinogenecity of welding, molybdenum trioxide, and indium tin oxide. Lancet Oncol 2017;18(5):581–2. [PubMed: 28408286]

[38]. IARC Working Group on the Evaluation of Carcinogenic Risks to Humans. Welding, molybdenum trioxide, and indium tin oxide In: Proceedings of IARC monographs on the evaluation of carcinogenic risks to humans. Lyon: IARC; 2018.

[39]. Sowards JW, Ramirez AJ, Dickinson DW, Lippold JC. Characterization of welding fume from SMAW electrodes-part II. Welding Journal 2010;89 (4):82s–90s.

[40]. 30 CFR 57.5001. Exposure limits for airborne contaminants. Safety and Health Standards – Underground Metal and Nonmetal Mines. Mine Safety and Health Administration. Code of Federal Regulations. Washington, DC, U.S. Government Printing Office, Office of the Federal Register.

[41]. MSHA. Metal Dusts, Fumes and Mists. Metal/Nonmetal Health Inspection Procedures Handbook. Mine Safety and Health Administration; 2006.

[43]. Johnson T, Caldow R, Pöcher A, Mirme A, Kittelson D. A new electrical mobility particle sizer spectrometer for engine exhaust particle measurements In: Proceedings of 2004 SAE world congress. Detroit, MI: SAE International; 2004.

[44]. Ahlvik P, Ntziachristos L, Keskinen J, Virtanen A. Real time measurement of diesel particle size distribution with an electric low pressure impactor In: Proceedings of 1998 SAE international congress and exposition; Detroit, MI: SAE International; 1998.

[45]. Keskinen J, Pietarinen K, Lehtimäki M. Electrical low pressure impactor. J Aerosol Sci 1992;23(4):353–60.

[46]. Giechaskiel B, Alföldy B, Drossinos Y. A metric for health effects studies of diesel exhaust particles. J Aerosol Sci 2009;40(8):639–51.

[47]. Brand P, Lenz K, Reisgen U, Kraus T. Number size distribution of fine and ultrafine fume particles from various welding processes. Ann Occup Hyg 2013;57(3):305–13. [PubMed: 23028013]

[48]. Bugarski AD, Janisko SJ, Cauda EG, Patts LD, Hummer JA, Westover C, et al. Aerosols and criteria gases in an underground mine that uses FAME biodiesel blends. Ann Occup Hyg 2014;58(8):971–82. [PubMed: 25060241]

[49]. Brouwer DH, Gijsbers JH, Lurvink MW. Personal exposure to ultrafine particles in the workplace: Exploring sampling techniques and strategies. Ann Occup Hyg 2004;48(5):439–53. [PubMed: 15240340]

[50]. Lamminen E, Reyes F, Vasquez Y, Teinilä K, Timonen H, Aurela M, Saarikoski S, Salonen RO, Linnainmaa M, Oyola P, Cubison MJ, Worsnop DR, Hillamo R. Real-time size distribution measurement of particulate matter in a mine In: Proceedings of 21st mining diesel emissions council conference. Toronto; 2015p.6–8.

[51]. Technologies Chimera. DistFitTM 2009 Users Guide. Chimera Technologies, Inc; 2009.

[52]. Noll JD, Timko RJ, McWilliams LJ, Hall P, Haney R. Sampling results of the improved SKC diesel particulate matter cassette. Journal of Occupational and Environmental Hygiene 2005;2(1):29–37. [PubMed: 15764521]

[53]. Birch ME. Monitoring diesel exhaust in the workplace NIOSH manual of analytical methods, 5th edition, Chapter DL. National Institute for Occupational Safety and Health, DHHS (NIOSH) Publication; 2016p.DL 1–41.

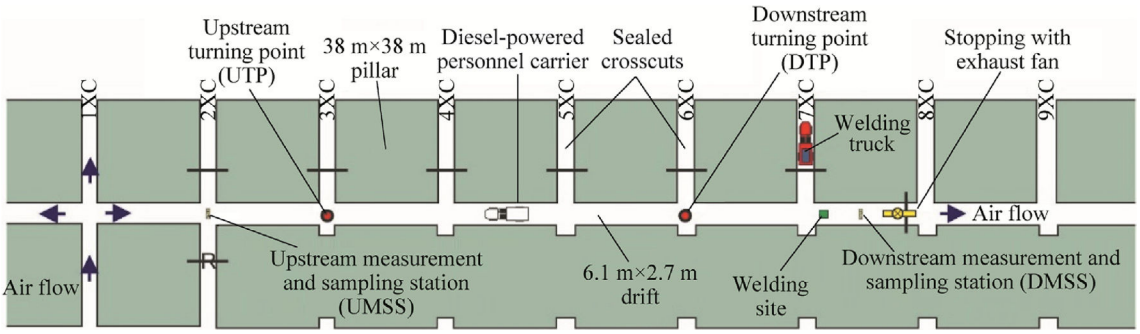

Fig. 1.
Layout of the test site.

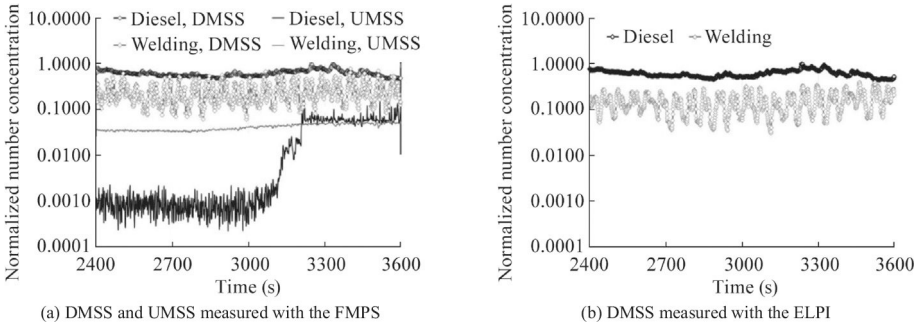

Fig. 2.

Normalized number concentrations of aerosols at the DMSS and UMSS measured with the FMPS and the DMSS measured with the ELPI.

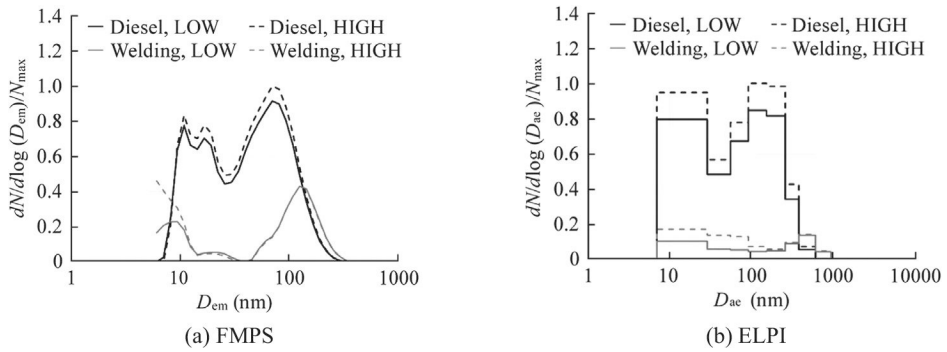

Fig. 3.

Normalized size distributions of aerosols at the DMSS at prevailing ventilation rates measured with FMPS and ELPI.

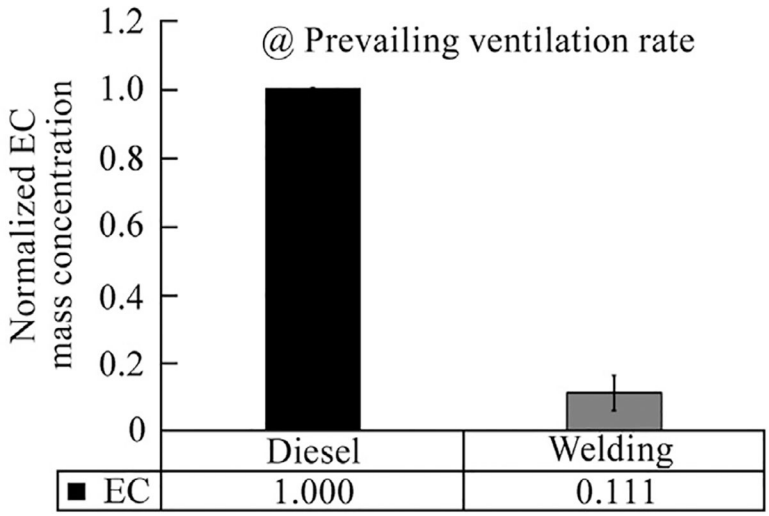

Fig. 4.
Average normalized net contributions to EC concentrations.

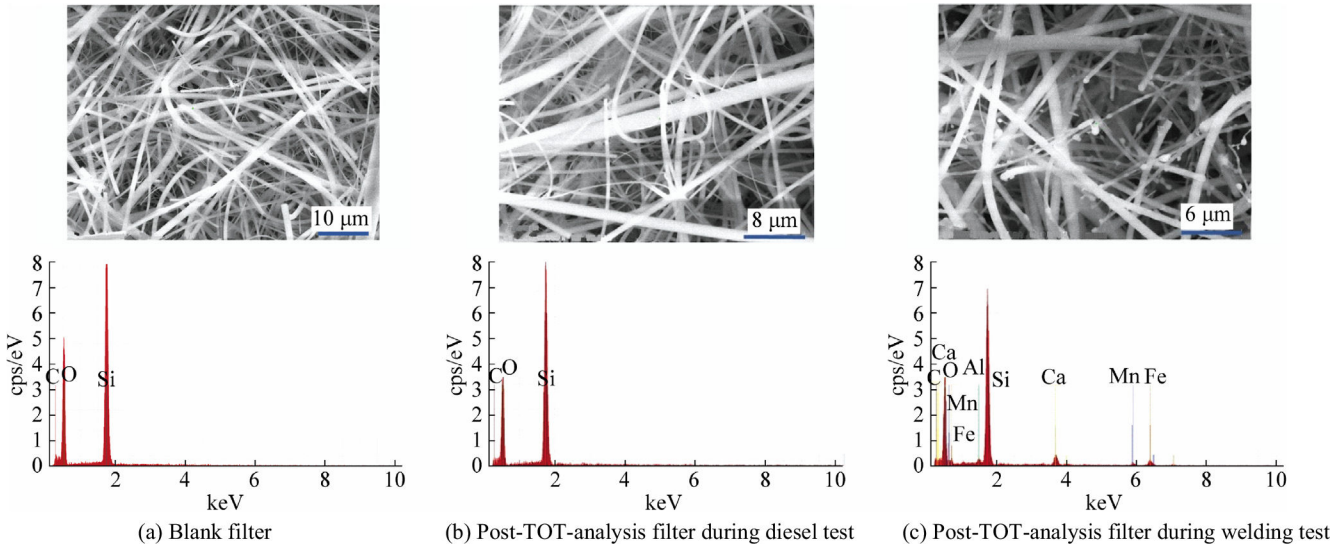

(a) Blank filter (b) Post-TOT-analysis filter during diesel test (c) Post-TOT-analysis filter during welding test

Fig. 5.

The SEM images and EDS spectra for QFF media punched out from blank filter, post-TOT-analysis filter collected during diesel test, and post-TOT-analysis filter collected during welding test.

Table 1

Diesel-powered vehicle used during the isolated zone study.

Parameter	Value
Equipment manufacturer and model	Duce III
Equipment type	Personnel carrier vehicle (LD nonpermissible)
Engine manufacturer and model	Cummins 4B3.3
Output (kW @ rpm)	48 @ 2000 rpm
MSHA approval number	7E-B093
MSHA ventilation rate (VR) (m^3/s)	1.65
MSHA particulate index (PI) (m^3/s)	3.78
EPA emissions standard	Pre-Tier

Table 2

Properties of the diesel fuel used for this study.

Fuel property	Test method	ULSD
Heat of combustion (MJ/kg)	ASTM D240	45.7
API gravity @ 15.6 °C (°API)	ASTM D1298	36.3
Cetane number	ASTM D613	46.2
Sulfur by ultraviolet (ppm)	ASTM D5453	11.0
Flash point, closed cup (°C)	ASTM D93	59.0

Table 3

Statistical parameters including electrical mobility count median diameters (CMD), spread(σ), and normalized total concentrations (NTC) for the lognormal curves fitted to the selected number distributions measured with the FMPS at the DMSS.

Test	Case	MODE 1			MODE 2			MODE 3		
		CMD (nm)	σ	NTC (#/cm^3)	CMD (nm)	σ	NTC (#/cm^3)	CMD (nm)	σ	NTC (#/cm^3)
Diesel only	Low	15	1.430	0.370	70	1.720	0.661	N/A	N/A	N/A
	High	15	1.430	0.399	70	1.720	0.719	N/A	N/A	N/A
Welding only	Low	7	1.820	0.134	64	1.140	0.011	137	1.420	0.072
	High	5	1.810	0.235	65	1.130	0.007	137	1.420	0.077

Int J Min Sci Technol. Author manuscript; available in PMC 2021 February 16.